Nano Research 2016, 9(7): 1948–1955
DOI 10.1007/s12274-016-1086-x
Research Article
ISSN 1998-0124
CN 11-5974/O4

Photophysical and electrical properties of organic waveguide nanorods of perylene-3,4,9,10-tetracarboxylic dianhydride

Yuyan Han[1,3], Wei Ning[1,3], Liang Cao[1,3], Xiaotao Xu[1], Tian Li[1], Fapei Zhang[1,3], Li Pi[1,3], Faqiang Xu[2] (✉), and Mingliang Tian[1,3,4] (✉)

[1] *High Magnetic Field Laboratory, Chinese Academy of Sciences, Hefei 230031, China*
[2] *National Synchrotron Radiation Laboratory, University of Science and Technology of China, 42 Hezuohua Road, Hefei 230029, China*
[3] *Hefei Science Center, Chinese Academy of Sciences, Hefei 230031, China*
[4] *Collaborative Innovation Center of Advanced Microstructures, Nanjing University, Nanjing 210093, China*

Received: 9 December 2015
Revised: 22 March 2016
Accepted: 25 March 2016

KEYWORDS
organic semiconductor, single crystalline nanorod, optical waveguide, photoluminescence, electrical conductivity

ABSTRACT

The single crystalline nanostructure of organic semiconductors provides a very promising class of materials for applications in modern optoelectronic devices. However, morphology control and optoelectronic property modulation of high quality single crystalline samples remain a challenge. Here, we report the morphology-controlled growth of single crystalline nanorod arrays of perylene-3,4,9,10-tetracarboxylic dianhydride (PTCDA). We demonstrate that, unlike PTCDA film, PTCDA nanorods exhibits optical waveguide features, enhanced absorption, and Frenkel excitation emission in the visible region. Additionally, we measured the electrical properties of PTCDA nanorods, including the conductivity along the growth direction of the nanorod, which is roughly 0.61 $S \cdot m^{-1}$ (much higher than that of pure crystalline PTCDA films).

1 Introduction

Because of their weak intermolecular forces (the π–π interaction, the charge-transfer (CT) interaction, the van der Waals force, and H-bands), organic semiconductors offer many unique advantages such as relative ease of chemical doping [1, 2], good processability [2], high reactivity [3], and high flexibility [4, 5]. These features make these materials complementary to their inorganic counterparts [6, 7] and allow them to be widely applied in the fabrication of modern optoelectronic devices, for example, organic light-emitting diodes [8, 9], organic field-effect transistors [10, 11], and organic solar cells [12].

Address correspondence to Mingliang Tian, tianml@hmfl.ac.cn; Faqiang Xu, fqxu@ustc.edu.cn

Previously, researchers have noted the size-dependent photophysical properties [13, 14] and the dielectric anisotropy of quasi-epitaxial crystalline organic semiconductor films [15, 16]. However, during the growth process of organic films, lattice mismatch originating from the substrate is inevitable and results in the generation of molecular disorder and increased grain boundaries. In the preparation process of one-dimensional (1D) organic nanomaterials using vapor deposition [17] or organic molecular beam deposition (OMBD) methods [18], once the initial nuclei are formed, the organic molecules will be epitaxially deposited on the nuclei and form single crystalline 1D nanomaterials with an oriented growth direction. Moreover, the vacuum environment can reduce doping in organic nanomaterials. These properties effectively decrease the amount of molecular disorder and grain boundaries [18]. Consequently, the photophysical and electrical properties of single crystalline organic 1D nanomaterials might be superior to those of quasi-epitaxial organic films. To our knowledge, the correlation between morphology and optoelectronic properties has not yet been systematically studied [13, 15].

To investigate the morphology-dependent photophysical and electrical properties of organic 1D nanomaterials, perylene-3,4,9,10-tetracarboxylic dianhydride (PTCDA) was selected as the model molecule. Because the PTCDA molecule has a planar structure, elements of perylene, and peripherally rich oxygen atoms (as shown in Fig. 1(a)), they favor π–π stacking between the layer-stacked molecules, which creates a basis of well-defined growth. The unique electronic structure of the planar π-electron system is usually used as the model example to investigate interfacial charge transfer dynamics [19, 20]; PTCDA crystalline films have already attracted attention and have been used in light-emitting diodes, where they were reported to improve charge injection efficiency at the anode [21, 22]. Herein, we successfully prepared vertically aligned PTCDA nanorod (NR) arrays and modulated their morphologies using the OMBD method. We found that the photophysical properties, especially the fluorescence feature, strongly depend on NR morphologies. We have also measured the current versus voltage (*I*–*V*) characteristics of individual NRs and found that the electrical conductivity along the epitaxial direction of PTCDA NRs was roughly 0.61 $S \cdot m^{-1}$, which is much higher than that of pure crystalline PTCDA films. Our experiments provide important information regarding the fabrication of optoelectronic devices based on π-conjugated planar organic semiconductors.

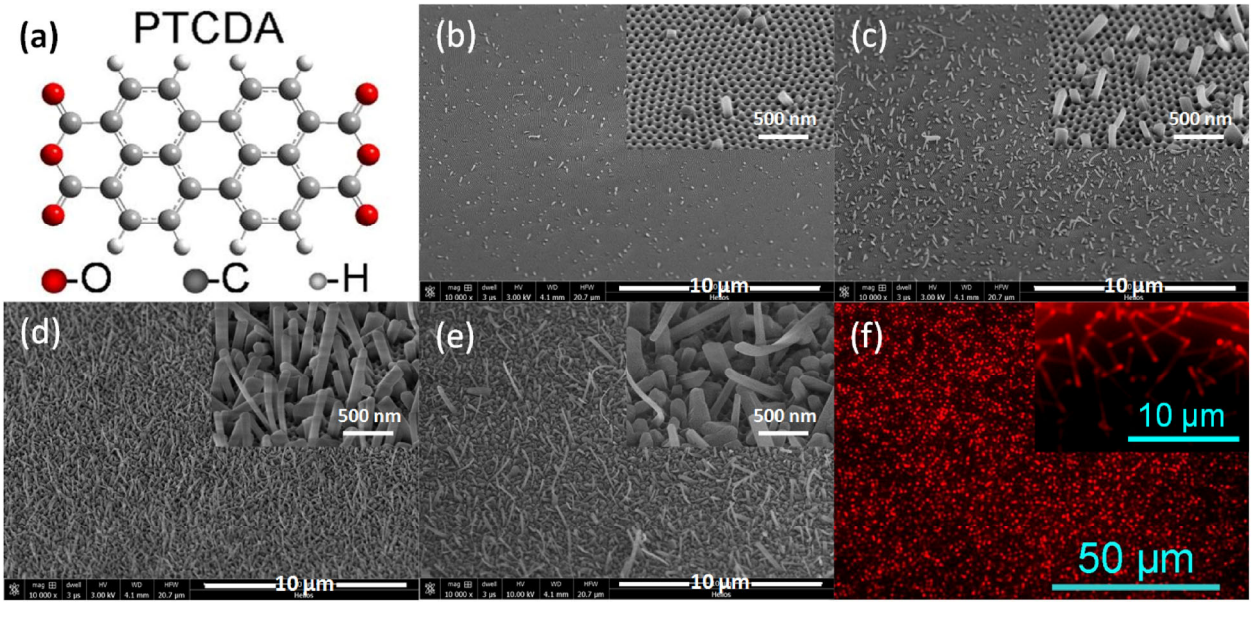

Figure 1 Chemical structure of PTCDA molecule (a). SEM images of PTCDA NR arrays prepared by setting t_g = 5 min (b), 20 min (c), 45 min (d), and 90 min (e); the insets show enlarged images. Top-view fluorescence microscopy images of the NR array grown for 90 min (f); the inset shows a side-view image of the NRs. All SEM images were taken at a 45° angle (tilted relative to the substrates).

2 Experimental

2.1 Preparation of PTCDA NR arrays

PTCDA NR arrays were prepared on anodic aluminum oxide (AAO) using the OMBD method; four growth times (t_g) of 5, 20, 45, and 90 min were selected. The substrate and the evaporator source temperatures were maintained at 280 and 385 ℃, respectively, during the growth processes. AAO was chosen as the substrate, because the surface of AAO possesses numerous array-arranged active sites with low curvature radius (i.e., high surface energy), which can favor nucleation of organic molecules [18, 23] and modulation of the aspect ratio of NRs. Detailed information regarding this process is presented (see Figs. S1 and S2 in the Electronic Supplementary Material (ESM)).

2.2 Characterization of morphologies and photophysical properties of PTCDA NR

Scanning electron microscopy (SEM) images and fluorescence images were obtained using an FEI NanoLab 600i SEM/FIB dual-beam system and IX 70 inverted fluorescence microscope, respectively. Ultraviolet visible (UV–Vis) absorption and photoluminescence (PL) spectra were acquired using a Shimadzu DUV-3700 spectrophotometer and a Jobin Yvon Fluorolog-3-21 fluorescence spectrophotometer, respectively. X-ray diffraction (XRD) patterns were collected using a Rigaku-TTR3 X-ray diffractometer.

2.3 Preparation and electrical characterization of NR devices

NR devices were fabricated using an FEI NanoLab 600i SEM/FIB dual-beam system. PTCDA NRs were first transferred onto a heavily doped Si substrate with a 500-nm SiO_2 dielectric layer. Then, platinum (Pt) stripes, acting as electrodes, were deposited on a randomly selected NR; further details regarding this process are given in Fig. S3 (in the ESM). The *I*–*V* characteristics were obtained using a probe station in a glove box at ambient temperature (argon atmosphere, H_2O < 0.1 ppm, O_2 < 0.1 ppm) and a Keithley 2612A digital source-meter.

3 Results and discussion

3.1 Morphology evolution of NRs with growth time

Figures 1(b)–1(e) show the SEM images of the PTCDA NR arrays grown for 5, 20, 45, and 90 min, respectively. In the early stage grown for 5 min, a layer of vertically aligned NRs was formed on the AAO surface with an average length of roughly 180 nm. Several longer NRs can also be seen in the low magnification image; they are related to the induced nucleation effect on the active sites (see Figs. S4 and S5 in the ESM). At the given substrate temperature of 280 ℃, active sites with relatively large curvature induce the preferable formation of initial nuclei on the AAO surface (which has a higher surface energy), which then epitaxially grow relative long NRs. The areas with relatively small curvature typically induce the laggard formation of initial nuclei, which grow into shorter NRs. At grown time (t_g) = 20 min, the NR width remains almost unchanged, whereas the NR length increases to approximately 800 nm, and the NR number increases. At t_g = 45 min, the NRs almost completely cover the AAO surface; NRs are roughly 2 μm long. For NRs grown for 90 min, the length of NRs reaches roughly 5 μm, and their width noticeably increases. SEM results suggest that both the length and the number of PTCDA NRs increase with t_g, and that some adjacent NRs combine together to form wider NRs.

3.2 Optical waveguide features

Figure 1(f) shows the top view of the PTCDA NR array, which was grown for 90 min on AAO under fluorescence excitation. The small bright lights emitting from the NR tips indicate good vertical growth of PTCDA NRs. To display the whole-body fluorescence feature, an image of the horizontally laid NRs is shown in the inset of Fig. 1(f). The fluorescence of PTCDA NR was brighter at the tips and weaker at the bodies, which is typical of the optical waveguide behavior reported by Zhao et al. and Takazawa et al. [23, 24].

Typically, layer stacking of planar molecules in single crystalline 1D nanostructures can produce optical waveguide features. Note that the majority of NRs located at the pore openings of the AAO have a

quasi-hexagonal cross-section, indicative of single crystalline morphology (see Figs. S6 and S7 in the ESM). To verify the crystal structure, we assessed the PTCDA NR array grown for 90 min by XRD, using Cu Kα radiation. Figure 2 shows the XRD result: Two peaks, at 26.60° and 27.66°, which are associated with (111) and (102) planes, respectively, can be identified. The peak at 27.66° is stronger, which indicates that the preferential orientation lattice plane in PTCDA NR is the (102) plane. The distance between the layer-stacked molecules is roughly 3.22 Å. The XRD result coincides with that of PTCDA nanostructures grown at roughly 290 ℃, as reported by S. Heutz et al. (see Fig. 3 in Ref. [13]). The π^*–π type transition in the PTCDA molecules combined with the transition of intermolecular CT excitons leads to strong fluorescence emission in the visible region [25–27]. Moreover, the PTCDA molecules stack layer-by-layer along the growth direction of crystalline NRs, and the distance (3.22 Å) between molecular stacks is smaller than both the other lattice constants and the size of PTCDA molecules [15, 16, 25]. This property causes strong interactions of π-electrons within the stacks [25]. Upon excitation, the resulting PL emission can be self-guided along the growth direction of the PTCDA NRs. Furthermore, in these crystals, the qualitative differences between Frenkel excitons (FEs) and CT excitons become small [25].

3.3 Photophysical properties of PTCDA NRs

To analyze the morphology-dependent photophysical properties of PTCDA NRs, we performed measurements of both UV–Vis absorption and PL spectra.

Figure 3(a) shows the UV–Vis absorption spectra of the annealed AAO, PTCDA film, and the PTCDA NR arrays. There is no absorption band in the spectrum of clean AAO; however, there is a sharp and isolated peak at 554 nm (2.24 eV), a broad feature between 400 and 535 nm (2.31–3.10 eV), and two high-energy peaks at 371 nm (3.34 eV) and 356 nm (3.48 eV), which appear once the PTCDA NR arrays or film are formed. The sharp feature at 554 nm (2.24 eV) originates from the CT-dominated charge-transfer-Frenkel mixing (CT-FE) mechanism (CT_{FE}), whereas the broad band between 400 and 535 nm (2.31–3.10 eV) originates from the FE-dominated CT-FE mechanism (FE_{CT}) [14, 25–27].

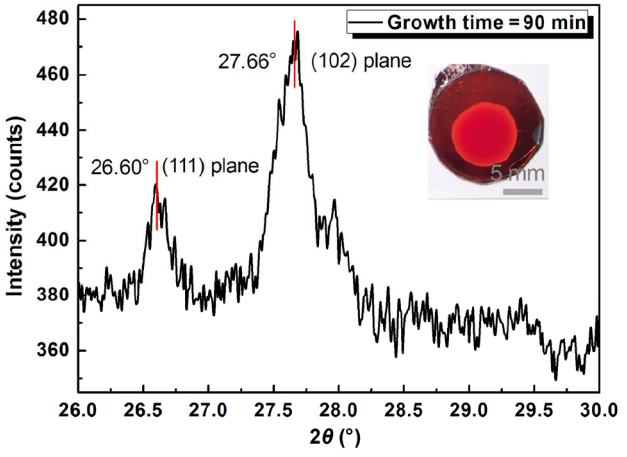

Figure 2 XRD pattern and optical image (inset) of AAO substrate for PTCDA NR array grown for 90 min.

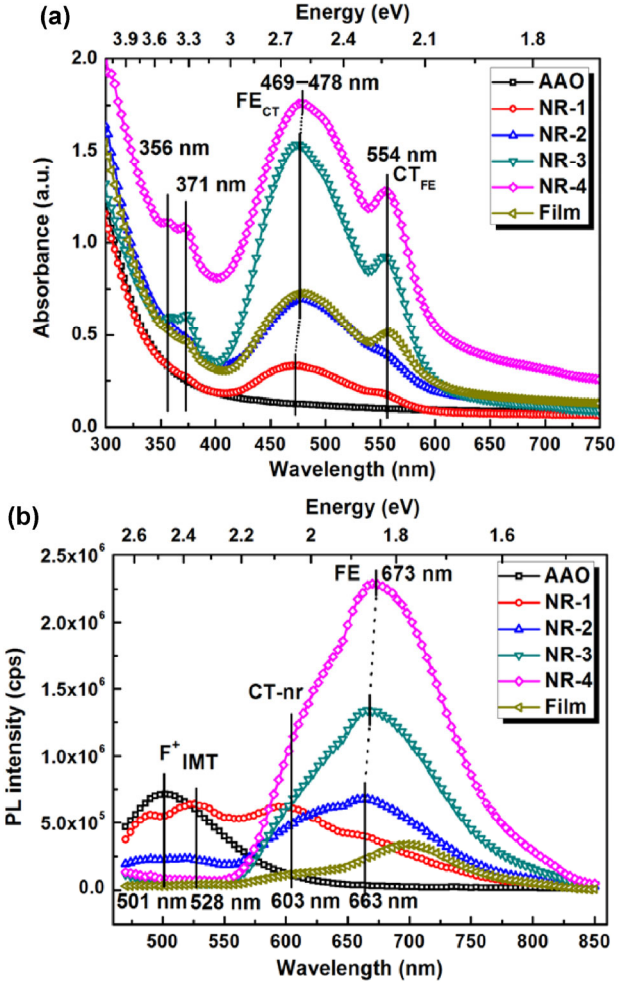

Figure 3 (a) UV–vis and (b) PL spectra of clean AAO, PTCDA film, and vertically aligned PTCDA NR arrays with different lengths. (NR-1 (180 nm), NR-2 (800 nm), NR-3 (2,000 nm), and NR-4 (5,000 nm) were prepared at t_g = 5, 20, 45, and 90 min, respectively; the excitation wavelength was 450 nm).

The two high energy peaks at 371 nm (3.34 eV) and 356 nm (3.48 eV) should arise from the intrinsic transition of PTCDA molecules. With increasing t_g, the center of the broad absorption band shows red-shift, whereas the positions of the other absorption peaks change slightly. The volume of PTCDA NRs increases with the growth time, and thus, induces an enhanced intermolecular overlap of PTCDA molecules, which subsequently results in the energy decrease (i.e., red-shift) of the FE_{CT} transition.

Figure 3(b) shows the PL spectra of annealed AAO, PTCDA film, and PTCDA NR arrays. One broad emission at 501 nm (2.48 eV) appears for clean AAO. Two comparable emissions at 528 nm (2.35 eV) and 603 nm (2.06 eV) appear for the shortest NR array. The emission at 663 nm (1.87 eV) becomes predominant as the average length of the NRs increases to 800 nm; its intensity continues to increase as the NR length increases further.

To better analyze the morphology-dependent PL spectra of PTCDA NRs, we consider the modulation mechanism of the dominant emission. It is known that the emission of AAO originates from an oxygen vacancy (F^+) [28, 29]. The *in situ* luminescence studies of ultrathin PTCDA film [30] suggest that the high energy emission at 528 nm (2.35 eV) for relatively short NR arrays derives from the isolated monomer transition (IMT); the emissions at 603 nm (2.06 eV) and 663 nm (1.87 eV) are, respectively, assigned to the transitions of the analogous non-relaxed state of the CT (CT-nr) de-excitation between the stacked PTCDA molecules in different unit cells and FE de-excitation within the same molecule [14, 27]. The continuous growth of PTCDA NRs enhances the overlap between PTCDA molecules, thereby reducing the number of monomer excitons and the energy of FE de-excitation. This results in a decrease in the intensity of the 528-nm (2.35 eV) band, and red-shift of the FE emission.

Here, we modulated both the morphology and the PL feature of PTCDA NRs. Because the intermolecular interactions that determine the concentrations and de-excitation energies of excitons can be tuned based on NR morphology, it is reasonable to believe that NR morphology is one of the decisive factors in tuning the PL feature.

3.4 Mechanisms of absorption and emission enhancement of PTCDA NR array

We note that although the coverage rate of PTCDA NR arrays on the AAO surface grown for 20 min is much less than that of PTCDA films (see Figs. S4 and S6 in the ESM), the absorbencies of PTCDA NR arrays and PTCDA films are almost equivalent. This result indicates that, in the visible region of 400 to 535 nm, the absorption efficiency of PTCDA NR arrays is much higher than that of PTCDA film.

Figure 4 qualitatively illustrates the mechanism of absorption enhancement of the PTCDA NR array. FE is one type of neutral excited state, in which the electron and hole are placed on the same molecule [25]. To generate FE in PTCDA NRs, the charge should transfer between donor and acceptor in the same PTCDA molecule plane. It is well known for light (i.e., electromagnetic waves), that the electric field vector ($\boldsymbol{E}_v$) is perpendicular to the propagation direction. In this work, PTCDA NRs were grown almost vertically on the AAO surface, and the incident light was projected vertically onto the AAO surface during the experimental measurement processes of absorption spectra. Consequently, $\boldsymbol{E}_v$ was, to a large extent, parallel to the molecular plane. This phenomenon resulted in enhanced absorption.

Furthermore, although the absorbance of the PTCDA NR array grown for 20 min was almost equal to that of the PTCDA film, the FE emission intensity of the PTCDA NR array was stronger, indicating enhanced FE emission of the PTCDA NR array. We believe that the enhanced FE emission originates primarily from the following three properties: high crystallinity, optical waveguide features, and vertical growth of PTCDA NRs. The high crystallinity reduces the concentration

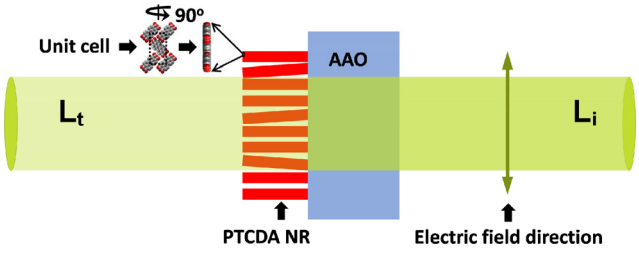

Figure 4 Diagram of absorption enhancement mechanism. (L_t: transmission light, L_i: incident light)

of crystal defects and grain boundaries in PTCDA NRs, which allows the excitonic species to diffuse further within the crystal NRs. The optical waveguide features cause the luminous energies to tend to propagate along the growth direction of the single crystalline NRs and emit primarily from the NR tips. The vertical growth of NRs favors fluorescent emission along the growth direction of the PTCDA NRs (i.e., normal to the AAO surface).

3.5 Electrical properties of PTCDA NRs

The layer-stacking of planar molecules in organic single crystals can also induce anisotropy in electrical conductivity. In quasi-epitaxial crystalline PTCDA films, the in-plane conductivity was found to be at least six orders of magnitude lower than the conductivity perpendicular to the film plane [16, 31]. To investigate the electrical performance in the growth direction of PTCDA NRs, we performed transport measurements on individual PTCDA NRs.

Figures 5(a) and 5(b), respectively, show the SEM image of the micro-device and the *I*–*V* curves of both PTCDA NRs and the SiO_2 dielectric layer as measured using the two-terminal technique. The *I*–*V* curve of the SiO_2 dielectric layer between the Pt electrode and the Si substrate shows insulating behavior, even when the voltage was swept from –100 to +100 V; the *I*–*V* curves of the PTCDA NRs measured at five different voltage ranges show good repeatability of electrical performance and confirm the typical semiconductor characteristics of PTCDA NRs. The current at a maximum voltage of 90 V is roughly 7.5×10^{-7} A; it can be calculated that the rated electric field intensity and the rated electric current density are roughly 1.58×10^{7} V·m^{-1} and 5.17×10^{6} A·m^{-2}, respectively.

The conductivity of PTCDA NR calculated based on the curve slope ($G = \Delta I/\Delta V \approx 0.155 \times 10^{-8}$ S) of the black short dashed lines (the fitted curve in the *I*–*V* curve's linear region) is roughly 0.61 S·m^{-1}, which is much higher than that of the pure crystalline PTCDA film [32]. This high conductivity should originate from both the strong π–π interaction between the layer-stacked PTCDA molecules (which favors charge transport perpendicular to the molecular planes) and the perfect crystalline structure of PTCDA NRs (which effectively avoids carrier scattering from defects and boundaries).

4 Conclusions

We prepared vertically aligned single crystalline PTCDA NR arrays using the OMBD method, and modulated the NR morphology by controlling the growth time. The π*–π transition and the intermolecular CT transition are believed to lead to strong PL emission in the visible region. Because of the strong π–electrons interactions between molecular stacks, the PL emission tends to be self-guided along the PTCDA NRs. The morphology slightly affects the intrinsic absorption features of PTCDA NRs, but strongly affects their PL features. Moreover, when the electrical field plane of the incident light is parallel to the molecular plane,

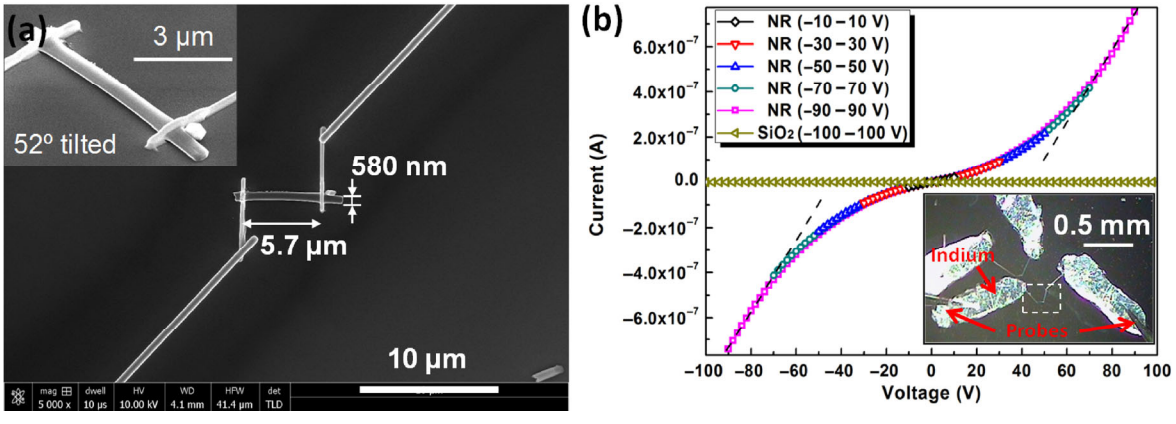

Figure 5 (a) SEM image of a single NR with Pt-electrodes deposited by FIB. The length, wide and thickness of the PTCDA NR are about 7.8 μm, 580 nm and 250 nm respectively, the distance of the inner two Pt electrodes is about 5.7 μm. (b) *I*–*V* curves of PTCDA NR on SiO_2 dielectric layer. (a) is located in the marked part in (b) inset which is the optical image of the device.

absorption enhancement occurs. The high degree of crystallinity, the optical waveguide features, and the vertical growth of the PTCDA NRs can result in enhanced FE emission along the growth direction of the PTCDA NRs. Specifically, the *I*–*V* characteristics are repeatable, because the rated electric field intensity and the rated current density are lower than 1.58×10^7 V·m^{-1} and 5.17×10^6 A·m^{-2}, respectively. The electrical conductivity of the PTCDA NRs is roughly 0.61 S·m^{-1}.

Acknowledgment

The authors thank Professor Lei Zhang for kind help in X-ray diffraction measurement, Mr. Fadi Li for assitance with the PL measurement, and Chiming Jin, Yan Liu and Wenshuai Gao for assitance with the device fabrication by FIB techniques. This work was supported by the National Natural Science Foundation of China (Nos. 11174294, 11374302, U1432251, 11574320, U1332139, 11575187 and 11574317), and the program of Users with Excellence, the Hefei Science Center of CAS and the CAS/SAFEA international partnership program for creative research teams of China.

Electronic Supplementary Material: Supplementary material (pretreatment of AAO and fabrication of PTCDA NR arrays; comparison between PTCDA nanostructures formed on AAO, glass and silicon substrates; micro-device preparation process; morphologies of AAO annealed and PTCDA film; the earlier stage of nucleation process; cross-sectional SEM images of PTCDA NR arrays; TEM and SAED results of PTCDA NR) is available in the online version of this article at http://dx.doi.org/10.1007/s12274-016-1086-x.

References

[1] Zhao, Y. S.; Fu, H. B.; Hu, F. Q.; Peng, A. D.; Yang, W. S.; Yao, J. N. Tunable emission from binary organic one-dimensional nanomaterials: An alternative approach to white-light emission. *Adv. Mater.* **2008**, *20*, 79–83.

[2] Peng, A. D.; Xiao, D. B.; Ma, Y.; Yang, W. S.; Yao, J. N. Tunable emission from doped 1,3,5-triphenyl-2-pyrazoline organic nanoparticles. *Adv. Mater.* **2005**, *17*, 2070–2073.

[3] Lim, S.-J.; An, B.-K.; Jung, S. D.; Chung, M.-A.; Park, S. Y. Photoswitchable organic nanoparticles and a polymer film employing multifunctional molecules with enhanced fluorescence emission and bistable photochromism. *Angew. Chem., Int. Ed.* **2004**, *43*, 6346–6350.

[4] Briseno, A. L.; Mannsfeld, S. C. B.; Lu, X. M.; Xiong, Y. J.; Jenekhe, S. A.; Bao, Z. N.; Xia, Y. N. Fabrication of field-effect transistors from hexathiapentacene single-crystal nanowires. *Nano Lett.* **2007**, *7*, 668–675.

[5] Kim, S.; Kwon, H.-J.; Lee, S.; Shim, H.; Chun, Y.; Choi, W.; Kwack, J.; Han, D.; Song, M.; Kim, S. et al. Low-power flexible organic light-emitting diode display device. *Adv. Mater.* **2011**, *23*, 3511–3516.

[6] Min, S.-Y.; Kim, T.-S.; Lee, Y.; Cho, H.; Xu, W. T.; Lee, T.-W. Organic nanowire fabrication and device applications. *Small* **2015**, *11*, 45–62.

[7] Zhao, Y. S.; Fu, H. B.; Peng, A. D.; Ma, Y.; Xiao, D. B.; Yao, J. N. Low-dimensional nanomaterials based on small organic molecules: Preparation and optoelectronic properties. *Adv. Mater.* **2008**, *20*, 2859–2876.

[8] Nikolaenko, A. E.; Cass, M.; Bourcet, F.; Mohamad, D.; Roberts, M. Thermally activated delayed fluorescence in polymers: A new route toward highly efficient solution processable OLEDs. *Adv. Mater.* **2015**, *27*, 7236–7240.

[9] Vasilopoulou, M.; Douvas, A. M.; Georgiadou, D. G.; Constantoudis, V.; Davazoglou, D.; Kennou, S.; Palilis, L. C.; Daphnomili, D.; Coutsolelos, A. G.; Argitis, P. Large work function shift of organic semiconductors inducing enhanced interfacial electron transfer in organic optoelectronics enabled by porphyrin aggregated nanostructures. *Nano Res.* **2014**, *7*, 679–693.

[10] Choi, K.; Nam, S.; Lee, Y.; Lee, M.; Jang, J.; Kim, S. J.; Jeong, Y. J.; Kim, H.; Bae, S.; Yoo, J.-B. et al. Reduced water vapor transmission rate of graphene gas barrier films for flexible organic field-effect transistors. *ACS Nano* **2015**, *9*, 5818–5824.

[11] Triet, N. M.; Trung, T. Q.; Hien, N. T. D.; Siddiqui, S.; Kim, D.-I.; Lee, J. C.; Lee, N.-E. A flexible magnetoelectric field-effect transistor with magnetically responsive nanohybrid gate dielectric layer. *Nano Res.* **2015**, *8*, 3421–3429.

[12] Homyak, P.; Liu, Y.; Liu, F.; Russel, T. P.; Coughlin, E. B. Systematic variation of fluorinated diketopyrrolopyrrole low bandgap conjugated polymers: Synthesis by direct arylation polymerization and characterization and performance in organic photovoltaics and organic field-effect transistors. *Macromolecules* **2015**, *48*, 6978–6986.

[13] Heutz, S.; Ferguson, A. J.; Rumbles, G.; Jones, T. S. Morphology, structure and photophysics of thin films of perylene-3,4,9,10-tetracarboxylic dianhydride. *Org. Electron.* **2002**, *3*, 119–127.

[14] Ferguson, A. J.; Jones, T. S. Photophysics of PTCDA and Me-PTCDI thin films: Effects of growth temperature. *J. Phys. Chem. B* **2006**, *110*, 6891–6898.

[15] Lovinger, A. J.; Forrest, S. R.; Kaplan, M. L.; Schmidt, P. H.; Venkatesan, T. Structural and morphological investigation of the development of electrical conductivity in ion-irradiated thin films of an organic material. *J. Appl. Phys.* **1984**, *55*, 476–482.

[16] Zang, D. Y.; So, F. F.; Forrest, S. R. Giant anisotropies in the dielectric properties of quasi-epitaxial crystalline organic semiconductor thin films. *Appl. Phys. Lett.* **1991**, *59*, 823–825.

[17] Zhao, Y. S.; Di, C.; Yang, W.; Yu, G.; Liu, Y.; Yao, J. Photoluminescence and electroluminescence from tris(8-hydroxyquinoline)aluminum nanowires prepared by adsorbent-assisted physical vapor deposition. *Adv. Funct. Mater.* **2006**, *16*, 1985–1991.

[18] Han, Y. Y.; Ning, W.; Du, H. F.; Yang, J. Y.; Wang, N.; Cao, L.; Li, F.; Zhang, F. P.; Xu, F. Q.; Tian, M. L. Preparation, optical and electrical properties of PTCDA nanostructures. *Nanoscale* **2015**, *7*, 17116–17121.

[19] Cao, L.; Wang, Y.-Z.; Zhong, J.-Q.; Han, Y.-Y.; Zhang, W.-H.; Yu, X.-J.; Xu, F.-Q.; Qi, D.-C.; Wee, A. T. S. Molecular orientation and site dependent charge transfer dynamics at PTCDA/TiO_2(110) interface revealed by resonant photoemission spectroscopy. *J. Phys. Chem. C* **2014**, *118*, 4160–4166.

[20] Cao, L.; Wang, Y. Z.; Zhong, J. Q.; Han, Y. Y.; Zhang, W. H.; Yu, X. J.; Xu, F. Q.; Qi, D.-C.; Wee, A. T. S. Electronic structure, chemical interactions and molecular orientations of 3,4,9,10-perylene-tetracarboxylic-dianhydride on TiO_2(110). *J. Phys. Chem. C* **2011**, *115*, 24880–24887.

[21] Chkoda, L.; Heske, C.; Sokolowski, M.; Umbach, E. Improved band alignment for hole injection by an interfacial layer in organic light emitting devices. *Appl. Phys. Lett.* **2000**, *77*, 1093–1095.

[22] Chu, X. B.; Guan, M.; Li, L. S.; Zhang, Y.; Zhang, F.; Li, Y. Y.; Zhu, Z. P.; Wang, B. Q.; Zeng, Y. P. Improved efficiency of organic/inorganic hybrid near-infrared light upconverter by device optimization. *ACS Appl. Mater. Interfaces* **2012**, *4*, 4976–4980.

[23] Zhao, Y. S.; Zhan, P.; Kim, J.; Sun, C.; Huang, J. X. Patterned growth of vertically aligned organic nanowire waveguide arrays. *ACS Nano* **2010**, *4*, 1630–1636.

[24] Takazawa, K.; Kitahama, Y.; Kimura, Y.; Kido, G. Optical waveguide self-assembled from organic dye molecules in solution. *Nano Lett.* **2005**, *5*, 1293–1296.

[25] Hoffmann, M.; Schmidt, K.; Fritz, T.; Hasche, T.; Agranovich, V. M.; Leo, K. The lowest energy Frenkel and charge-transfer excitons in quasi-one-dimensional structures: Application to MePTCDI and PTCDA crystals. *Chem. Phys.* **2000**, *258*, 73–96.

[26] Wagner, H. P.; DeSilva, A.; Kampen, T. U. Exciton emission in PTCDA films and PTCDA/Alq_3 multilayers. *Phys. Rev. B* **2004**, *70*, 235201.

[27] Gangilenka, V. R.; Titova, L. V.; Smith, L. M.; Wagner, H. P.; DeSilva, L. A. A.; Gisslén, L.; Scholz, R. Selective excitation of exciton transitions in PTCDA crystals and films. *Phys. Rev. B* **2010**, *81*, 155208.

[28] Du, Y.; Cai, W. L.; Mo, C. M.; Chen, J.; Zhang, L. D.; Zhu, X. G. Preparation and photoluminescence of alumina membranes with ordered pore arrays. *Appl. Phys. Lett.* **1999**, *74*, 2951–2953.

[29] Sun, X. Y.; Xu, F. Q.; Li, Z. M.; Zhang, W. H. Photoluminescence properties of anodic alumina membranes with ordered nanopore arrays. *J. Lumines.* **2006**, *121*, 588–594.

[30] Schlettwein, D.; Back, A.; Schilling, B.; Fritz, T.; Armstrong, N. R. Ultrathin films of perylenedianhydride and perylenebis(dicarboximide) dyes on (001) alkali halide surfaces. *Chem. Mater.* **1998**, *10*, 601–612.

[31] Schmidt, R.; Oh, J. H.; Sun, Y.-S.; Deppisch, M.; Krause, A.-M.; Radacki, K.; Braunschweig, H.; Könemann, M.; Erk, P.; Bao, Z. et al. High-performance air-stable n-channel organic thin film transistors based on halogenated perylene bisimide semiconductors. *J. Am. Chem. Soc* **2009**, *131*, 6215–6228.

[32] Forrest, S. R.; Kaplan, M. L.; Schmidt, P. H.; Venkatesan, T.; Lovinger, A. J. Large conductivity changes in ion beam irradiated organic thin films. *Appl. Phys. Lett.* **1982**, *41*, 708–710.